

Improved measurement of $\bar{B}^0 \rightarrow D_s^- D^+$ and search for $\bar{B}^0 \rightarrow D_s^+ D_s^-$ at Belle

A. Zupanc,¹⁵ K. Abe,⁹ K. Abe,⁴⁵ H. Aihara,⁴⁷ D. Anipko,¹ K. Arinstein,¹ V. Aulchenko,¹ T. Aushev,^{19,14} S. Bahinipati,³ A. M. Bakich,⁴² E. Barberio,²² U. Bitenc,¹⁵ I. Bizjak,¹⁵ S. Blyth,²⁵ A. Bondar,¹ A. Bozek,²⁸ M. Bračko,^{9,21,15} T. E. Browder,⁸ M.-C. Chang,⁴ P. Chang,²⁷ Y. Chao,²⁷ K.-F. Chen,²⁷ W. T. Chen,²⁵ B. G. Cheon,⁷ R. Chistov,¹⁴ S.-K. Choi,⁶ Y. Choi,⁴¹ Y. K. Choi,⁴¹ J. Dalseno,²² M. Dash,⁵¹ A. Drutskoy,³ S. Eidelman,¹ S. Fratina,¹⁵ N. Gabyshev,¹ A. Go,²⁵ B. Golob,^{20,15} H. Ha,¹⁷ J. Haba,⁹ T. Hara,³³ H. Hayashii,²⁴ M. Hazumi,⁹ D. Heffernan,³³ T. Hokuue,²³ Y. Hoshi,⁴⁵ W.-S. Hou,²⁷ Y. B. Hsiung,²⁷ T. Iijima,²³ K. Ikado,²³ K. Inami,²³ A. Ishikawa,⁴⁷ H. Ishino,⁴⁸ R. Itoh,⁹ Y. Iwasaki,⁹ H. Kaji,²³ P. Kapusta,²⁸ H. Kawai,² T. Kawasaki,³⁰ H. Kichimi,⁹ H. J. Kim,¹⁸ Y. J. Kim,⁵ K. Kinoshita,³ S. Korpar,^{21,15} P. Križan,^{20,15} P. Krokovny,⁹ R. Kulasiri,³ R. Kumar,³⁴ Y.-J. Kwon,⁵² M. J. Lee,³⁹ T. Lesiak,²⁸ A. Limosani,⁹ S.-W. Lin,²⁷ D. Liventsev,¹⁴ G. Majumder,⁴³ F. Mandl,¹² T. Matsumoto,⁴⁹ S. McOnie,⁴² T. Medvedeva,¹⁴ W. Mitaroff,¹² K. Miyabayashi,²⁴ H. Miyake,³³ H. Miyata,³⁰ Y. Miyazaki,²³ R. Mizuk,¹⁴ G. R. Moloney,²² E. Nakano,³² M. Nakao,⁹ H. Nakazawa,²⁵ Z. Natkaniec,²⁸ S. Nishida,⁹ O. Nitoh,⁵⁰ S. Ogawa,⁴⁴ T. Ohshima,²³ S. Okuno,¹⁶ Y. Onuki,³⁶ H. Ozaki,⁹ P. Pakhlov,¹⁴ G. Pakhlova,¹⁴ C. W. Park,⁴¹ R. Pestotnik,¹⁵ L. E. Piilonen,⁵¹ Y. Sakai,⁹ N. Satoyama,⁴⁰ T. Schietinger,¹⁹ O. Schneider,¹⁹ C. Schwanda,¹² R. Seidl,^{10,36} K. Senyo,²³ M. E. Sevir,²² M. Shapkin,¹³ H. Shibuya,⁴⁴ B. Shwartz,¹ J. B. Singh,³⁴ A. Somov,³ N. Soni,³⁴ S. Stanić,³¹ M. Starič,¹⁵ H. Stoeck,⁴² K. Sumisawa,⁹ T. Sumiyoshi,⁴⁹ S. Suzuki,³⁷ F. Takasaki,⁹ K. Tamai,⁹ M. Tanaka,⁹ G. N. Taylor,²² Y. Teramoto,³² X. C. Tian,³⁵ I. Tikhomirov,¹⁴ K. Trabelsi,⁹ T. Tsukamoto,⁹ S. Uehara,⁹ K. Ueno,²⁷ S. Uno,⁹ Y. Ushiroda,⁹ Y. Usov,¹ G. Varner,⁸ S. Villa,¹⁹ C. H. Wang,²⁶ Y. Watanabe,⁴⁸ E. Won,¹⁷ Q. L. Xie,¹¹ A. Yamaguchi,⁴⁶ Y. Yamashita,²⁹ M. Yamauchi,⁹ Y. Yusa,⁵¹ C. C. Zhang,¹¹ Z. P. Zhang,³⁸ V. Zhilich,¹ and V. Zhulanov¹

(The Belle Collaboration)

¹*Budker Institute of Nuclear Physics, Novosibirsk*

²*Chiba University, Chiba*

³*University of Cincinnati, Cincinnati, Ohio 45221*

⁴*Department of Physics, Fu Jen Catholic University, Taipei*

⁵*The Graduate University for Advanced Studies, Hayama*

⁶*Gyeongsang National University, Chinju*

⁷*Hanyang University, Seoul*

⁸*University of Hawaii, Honolulu, Hawaii 96822*

⁹*High Energy Accelerator Research Organization (KEK), Tsukuba*

¹⁰*University of Illinois at Urbana-Champaign, Urbana, Illinois 61801*

¹¹*Institute of High Energy Physics, Chinese Academy of Sciences, Beijing*

¹²*Institute of High Energy Physics, Vienna*

¹³*Institute of High Energy Physics, Protvino*

¹⁴*Institute for Theoretical and Experimental Physics, Moscow*

¹⁵*J. Stefan Institute, Ljubljana*

¹⁶*Kanagawa University, Yokohama*

¹⁷*Korea University, Seoul*

¹⁸*Kyungpook National University, Taegu*

¹⁹*Swiss Federal Institute of Technology of Lausanne, EPFL, Lausanne*

²⁰*University of Ljubljana, Ljubljana*

²¹*University of Maribor, Maribor*

²²*University of Melbourne, School of Physics, Victoria 3010*

²³*Nagoya University, Nagoya*

²⁴*Nara Women's University, Nara*

²⁵*National Central University, Chung-li*

²⁶*National United University, Miao Li*

²⁷*Department of Physics, National Taiwan University, Taipei*

²⁸*H. Niewodniczanski Institute of Nuclear Physics, Krakow*

²⁹*Nippon Dental University, Niigata*

³⁰*Niigata University, Niigata*

³¹University of Nova Gorica, Nova Gorica

³²Osaka City University, Osaka

³³Osaka University, Osaka

³⁴Panjab University, Chandigarh

³⁵Peking University, Beijing

³⁶RIKEN BNL Research Center, Upton, New York 11973

³⁷Saga University, Saga

³⁸University of Science and Technology of China, Hefei

³⁹Seoul National University, Seoul

⁴⁰Shinshu University, Nagano

⁴¹Sungkyunkwan University, Suwon

⁴²University of Sydney, Sydney, New South Wales

⁴³Tata Institute of Fundamental Research, Mumbai

⁴⁴Toho University, Funabashi

⁴⁵Tohoku Gakuin University, Tagajo

⁴⁶Tohoku University, Sendai

⁴⁷Department of Physics, University of Tokyo, Tokyo

⁴⁸Tokyo Institute of Technology, Tokyo

⁴⁹Tokyo Metropolitan University, Tokyo

⁵⁰Tokyo University of Agriculture and Technology, Tokyo

⁵¹Virginia Polytechnic Institute and State University, Blacksburg, Virginia 24061

⁵²Yonsei University, Seoul

(Dated: August 25, 2019)

We reconstruct $\bar{B}^0 \rightarrow D_s^- D^+$ decays using a sample of 449×10^6 $B\bar{B}$ pairs recorded by the Belle experiment, and measure the branching fraction to be $\mathcal{B}(\bar{B}^0 \rightarrow D_s^- D^+) = [7.5 \pm 0.2(\text{stat}) \pm 0.8(\text{syst}) \pm 0.8(\mathcal{B}'\text{s})] \times 10^{-3}$. A search for the related decay $\bar{B}^0 \rightarrow D_s^+ D_s^-$ is also performed. Since we observe no statistically significant signal an upper limit on the branching fraction is set at 3.6×10^{-5} (90% C.L.).

PACS numbers: 13.25.Hw, 14.40.Nd

I. INTRODUCTION

Several decay modes of B mesons with a D_s^+ in the final state have been measured at the B -factories. The amplitudes governing these decays are interesting because none of the constituent flavors of the D_s^+ are present in the initial state. For example, the decays $\bar{B}^0 \rightarrow D_s^+ K^-$ [1, 2] and $\bar{B}^0 \rightarrow D_{s0}^*(2317)^+ K^-$ [3], observed with branching fractions in the range $10^{-5} - 10^{-4}$, can proceed via a $b\bar{d} \rightarrow c\bar{u}$ W -exchange diagram. Here we study the related decays $\bar{B}^0 \rightarrow D_s^+ D_s^-$ and $\bar{B}^0 \rightarrow D_s^- D^+$. The former proceeds via Cabibbo-suppressed W -exchange and has not yet been observed; theoretical calculations predict a branching fraction ranging from $\sim 8 \times 10^{-5}$ [4] up to $\sim 3 \times 10^{-4}$ [5]. The latter of the two above decays proceeds via a Cabibbo-favored tree diagram; the ratio of its branching fraction to that for $\bar{B}^0 \rightarrow D^+ \pi^-$ can be used to test the factorization hypothesis for exclusive non-leptonic decays of B mesons [6]. However, previous measurements of $\mathcal{B}(\bar{B}^0 \rightarrow D_s^+ D^-)$ [7, 8, 9, 10] have large uncertainties, which limit the usefulness of this method at present.

In this paper we report an improved measurement of $\bar{B}^0 \rightarrow D_s^- D^+$ decays and a search for $\bar{B}^0 \rightarrow D_s^+ D_s^-$ decays with the Belle detector [11] at the KEKB asymmetric-energy e^+e^- collider [12]. Charge conjugate modes are implied throughout this paper. The results are based on a 414 fb^{-1} data sample collected at the

center-of-mass (CM) energy of the $\Upsilon(4S)$ resonance, corresponding to $(449.3 \pm 5.7) \times 10^6$ $B\bar{B}$ pairs. We assume equal production of $B^0\bar{B}^0$ and B^+B^- pairs. To study backgrounds, we use a Monte Carlo (MC) simulated sample [13] of $\Upsilon(4S) \rightarrow B\bar{B}$ events and continuum events, $e^+e^- \rightarrow q\bar{q}$ ($q = u, d, s$ and c quarks).

The Belle detector is a large-solid-angle magnetic spectrometer that consists of a multi-layer silicon vertex detector (SVD), a 50-layer central drift chamber (CDC), an array of aerogel threshold Cherenkov counters (ACC), a barrel-like arrangement of time-of-flight scintillation counters (TOF), and an electromagnetic calorimeter (ECL) comprised of CsI(Tl) crystals located inside a superconducting solenoid coil that provides a 1.5 T magnetic field. An iron flux-return located outside of the coil is instrumented to detect K_L^0 mesons and to identify muons (KLM). The detector is described in detail in Ref. [11]. Two different inner detector configurations were used. For the first 152 million $B\bar{B}$ pairs, a 2.0 cm radius beampipe and a 3-layer silicon vertex detector were used; for the latter 297 million $B\bar{B}$ pairs, a 1.5 cm radius beampipe, a 4-layer silicon detector and a small-cell inner drift chamber were used [14].

II. RECONSTRUCTION

Charged tracks are selected with loose requirements on their impact parameters relative to the interaction point (IP) and the transverse momentum of the tracks. For charged particle identification (PID) we combine information from the CDC, TOF and ACC counters into a likelihood ratio $\mathcal{L}(K)/(\mathcal{L}(K) + \mathcal{L}(\pi))$ [15]. A selection imposed on this ratio results in a typical kaon (pion) identification efficiency ranging from 92% to 97% (94% to 98%) for various decay modes, while 2% to 15% (4% to 8%) of kaon (pion) candidates are misidentified pions (kaons).

We use the $D_s^- \rightarrow \phi\pi^-$, $K^{*0}K^-$ and $K_S^0K^-$ modes to reconstruct D_s^- mesons and $D^+ \rightarrow K^+K^-\pi^+$, $K^-\pi^+\pi^+$, and $K_S^0\pi^+$ for the D^+ mesons, where the ϕ , K^{*0} and K_S^0 decay to K^+K^- , $K^+\pi^-$ and $\pi^-\pi^+$, respectively. Combinations of oppositely-charged kaons with $|m_\phi - M_{K^+K^-}| < 20$ MeV/ c^2 and of oppositely-charged kaons and pions with $|m_{K^{*0}} - M_{K^+\pi^-}| < 85$ MeV/ c^2 , originating from a common vertex, are retained as ϕ and K^{*0} candidates, where m_ϕ and $m_{K^{*0}}$ are the nominal masses of the two mesons [16]. Neutral kaons (K_S^0) are reconstructed using pairs of oppositely-charged tracks that have an invariant mass within 30 MeV/ c^2 of the nominal K^0 mass, and originate from a common vertex, displaced from the IP. All $D_{(s)}$ candidates with invariant masses within a 4σ (4.5σ) interval around the nominal D_s (D) mass are considered for further analysis, where D_s (D) signal resolutions (σ) range from 3.6 MeV/ c^2 to 4.2 MeV/ c^2 (3.7 MeV/ c^2 to 4.1 MeV/ c^2). A decay vertex fit with a mass constraint is applied to the selected $D_{(s)}$ candidates to improve their momentum resolution. For the decay $\bar{B}^0 \rightarrow D_s^+D_s^-$ we also add an additional constraint on the value of the cosine of a helicity angle, $|\cos\theta_h| > 0.05$ (0.25) for the $D_s^- \rightarrow \phi\pi^-$ ($K^{*0}K^-$) decay mode, where θ_h is defined as the angle between the direction of the D_s^- and the K^+ originating from the vector-meson (ϕ or K^{*0}) in the vector-meson rest frame. The distribution in $\cos\theta_h$ is expected to be proportional to $\cos^2\theta_h$ for the signal and uniform for the combinatorial background.

Pairs of D_s^- and $D_{(s)}^+$ meson candidates are combined to form \bar{B}^0 meson candidates. These are identified by their CM energy difference, $\Delta E = E_B^{\text{CM}} - E_{\text{beam}}^{\text{CM}}$, and the beam-energy constrained mass, $M_{\text{bc}} = \sqrt{(E_{\text{beam}}^{\text{CM}})^2 - (p_B^{\text{CM}})^2}$, where $E_{\text{beam}}^{\text{CM}} = \sqrt{s}/2$ is the CM beam energy and E_B^{CM} and p_B^{CM} are the reconstructed energy and momentum of the B meson candidate in the CM frame. The signal region is $5.272 \text{ GeV}/c^2 \leq M_{\text{bc}} \leq 5.285 \text{ GeV}/c^2$ for the $\bar{B}^0 \rightarrow D_s^-D^+$, and $5.274 \text{ GeV}/c^2 \leq M_{\text{bc}} \leq 5.284 \text{ GeV}/c^2$ and $|\Delta E| \leq 0.013 \text{ GeV}$ for the $\bar{B}^0 \rightarrow D_s^+D_s^-$ decays.

To suppress the large combinatorial background dominated by the two-jet-like $e^+e^- \rightarrow q\bar{q}$ continuum process, variables characterizing the event topology are used. We require the ratio of the second to zeroth Fox-Wolfram mo-

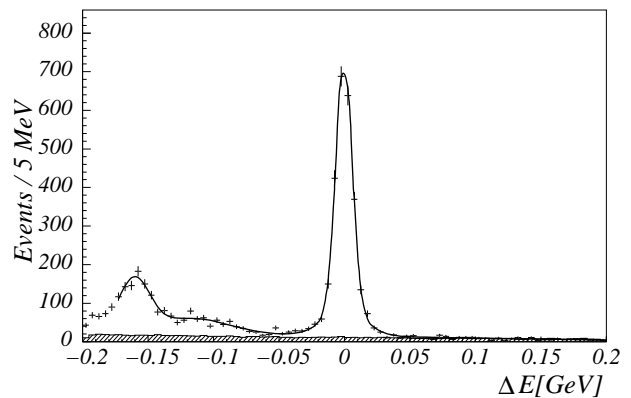


FIG. 1: ΔE distribution for reconstructed $\bar{B}^0 \rightarrow D_s^- D^+$ events in the M_{bc} signal region. The curve shows the result of the fit. The normalized distribution for the events in the sidebands of both D_s and D invariant masses is shown as the hatched histogram.

ments [17], $R_2 < 0.3$ and the thrust value of the event, $T < 0.8$. Simulation shows that this selection retains more than 95% of $B\bar{B}$ events and rejects about 55% of $c\bar{c}$ events and 65% of $u\bar{u}$, $d\bar{d}$ and $s\bar{s}$ events.

The above selection criteria and signal regions are determined by maximizing the figure of merit (FoM), $S/\sqrt{S+B}$, where S and B are the numbers of signal and background events determined from MC. For optimization of the FoM we assume $\mathcal{B}(\bar{B}^0 \rightarrow D_s^+D_s^-) = 2 \times 10^{-4}$.

The fraction of events with more than one $\bar{B}^0 \rightarrow D_s^-D^+$ ($\bar{B}^0 \rightarrow D_s^+D_s^-$) candidate is 4.9% (2.8%). As the best candidate we select the one with the minimal $\chi^2 = \chi^2(D_s^-) + \chi^2(D_{(s)}^+)$ value, where $\chi^2(D_s^-)$ and $\chi^2(D_{(s)}^+)$ are χ^2 's of the mass-constrained vertex fit.

III. $\bar{B}^0 \rightarrow D_s^- D^+$ DECAYS

The ΔE distribution of events in the M_{bc} signal region, obtained after applying all selection criteria described above is shown in Fig. 1. Apart from the signal peak at $\Delta E = 0$, contributions from two other specific decay modes were identified using the MC: $\bar{B}^0 \rightarrow D_s^{*-}D^+$ and $\bar{B}^0 \rightarrow D_s^-D^{*+}$. These events cluster around $\Delta E = -0.16 \text{ GeV}$ and -0.10 GeV due to the unreconstructed π^0 or γ from the $D_{(s)}^*$ meson.

The ΔE distribution is described by two Gaussians with the same mean for the signal, two Gaussians for the $\bar{B}^0 \rightarrow D_s^{*-}D^+$, $D_s^-D^{*+}$ background events, and a linear function for the rest of the background. The normalizations, positions and widths of the Gaussians are free parameters of the binned likelihood fit. The solid line in Fig. 1 shows the result of the fit. The positions and widths of the $\bar{B}^0 \rightarrow D_s^{*-}D^+$, $D_s^-D^{*+}$ background components agree with the values expected from the MC. In addition, we perform separate fits to the ΔE distri-

butions for each D_s decay mode using the same function with the widths and means of all four Gaussian functions fixed to the values obtained by the overall ΔE fit.

We use events in the D_s and D meson invariant mass sidebands in order to check for peaking backgrounds. For this check the masses of D_s and D candidates are not constrained to their nominal masses. The $D(D_s)$ invariant mass sidebands are ± 200 MeV/ c^2 intervals around $D(D_s)$ nominal mass, excluding the $D(D_s)$ signal region. Due to common final states used to reconstruct D and D_s candidates we exclude the $D_s(D)$ signal regions and a ± 27 MeV/ c^2 D^{*+} mass region from $D(D_s)$ sidebands. The ΔE and M_{bc} distributions obtained by simultaneously using events in the sidebands of both the D and D_s mesons are in agreement with the observed combinatorial background under the $\overline{B}^0 \rightarrow D_s^- D^+$ signal. A significant signal is present only in the D_s sideband, for D_s 's reconstructed in the $D_s^- \rightarrow K^{*0} K^-$ decay mode. This is due to the three-body $\overline{B}^0 \rightarrow D^+ K^{*0} K^-$ decay, reported in Ref. [18]. The fraction of these events in the signal peak was evaluated by fitting the ΔE distribution in the D_s sideband. We observe no peaking background when using the D mass sideband. The signal in Fig. 1 also includes contributions from $D_s^+ \rightarrow K^+ K^- \pi^+$, $f_0(980)\pi^+$ and $\overline{K}_0^*(1430)^0 K^+$, which all have a common final state, as well as a small contribution (0.4%) from $D^+ \rightarrow K^- \pi^+ \pi^+$ decays, where one of the π^+ decays in-flight to a μ^+ and ν_μ and the μ^+ is misidentified as the π^+ . We evaluate these fractions using simulated events. The contribution of these decays is around five times larger than the contribution of $\overline{B}^0 \rightarrow D^+ K^{*0} K^-$ decays. We take into account the relative contributions of individual D_s and D decay modes and determine the overall fraction of peaking background events (r) to be $(11.3 \pm 2.6)\%$. The uncertainty includes the statistical uncertainty in D_s sideband fits, non-uniformity of $M(K^{*0} K^-)$ in $\overline{B}^0 \rightarrow D^+ K^{*0} K^-$ decays, limited MC statistics and uncertainties in the corresponding branching fractions [16].

The signal yield for $\overline{B}^0 \rightarrow D_s^- D^+$ is thus $N = (1 - r)N_{\text{peak}} = 2230 \pm 56(\text{stat})$, where N_{peak} is the number of events in the signal peak obtained from the fit to the ΔE distribution (Fig. 1).

IV. $\overline{B}^0 \rightarrow D_s^+ D_s^-$ DECAYS

The ΔE distribution for $\overline{B}^0 \rightarrow D_s^+ D_s^-$ decays obtained after applying all selection criteria described above is shown in Fig. 2(a). The expected width of the narrower signal Gaussian, which describes 82% of the events, is 5.8 MeV. This value is obtained from the MC sample and rescaled by a factor obtained after a comparison of parameters from $\overline{B}^0 \rightarrow D_s^- D^+$ data and MC samples. The ΔE signal region includes around 89% of the signal.

While the ΔE distribution of the combinatorial background is well described by a first order polynomial, there is a significant cross-feed contribution from $\overline{B}^0 \rightarrow D_s^- D^+$, $D_s^{*-} D^+$, and $D_s^- D^{*+}$ decays, where the D^+ de-

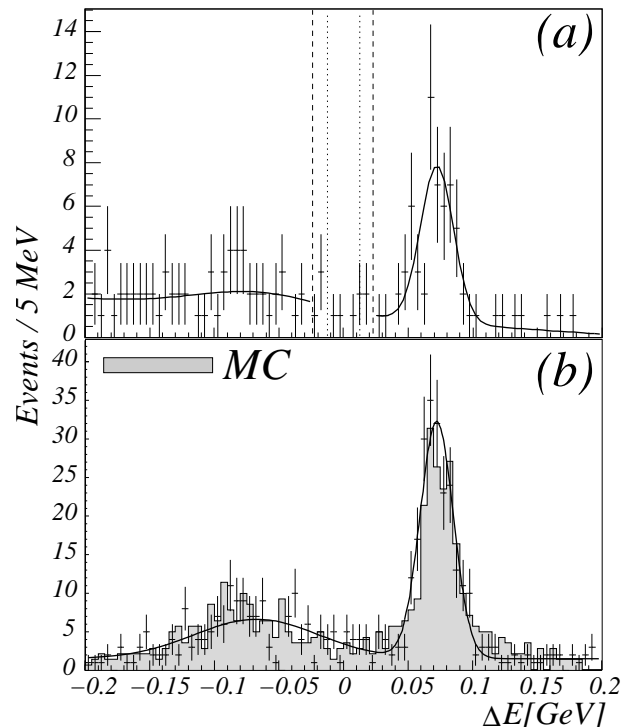


FIG. 2: (a) ΔE distribution for the $\overline{B}^0 \rightarrow D_s^+ D_s^-$ decay mode. Two vertical dashed lines show the interval excluded from the fit, as described in the text, and two dotted lines show the ΔE signal region. (b) ΔE distribution for reconstructed events obtained by inverting the kaon identification requirements in data and in the MC sample.

cays into a $K^- \pi^+ \pi^+$ or $\overline{K}^0 \pi^+$ final state and one of the pions is misidentified as a kaon. Figure 2(b) shows the ΔE distribution of these cross-feed events, as obtained in both data and MC samples by selecting one of the kaon tracks in the D_s decay chain with a pion PID requirement. Events peaking around 0.075 GeV are due to $\overline{B}^0 \rightarrow D_s^- D^+$ decays, while the events clustering around -0.1 GeV are due to $\overline{B}^0 \rightarrow D_s^{*-} D^+$ and $\overline{B}^0 \rightarrow D_s^- D^{*+}$ decays without a reconstructed π^0 or a photon. The ΔE distribution of cross-feed events is described by the sum of two Gaussian functions and a constant. The solid line in Fig. 2(b) shows the result of the fit. The widths and means of the two Gaussian functions are statistically consistent with the values obtained from MC.

The expected number of background events populating the ΔE signal region is determined by a binned likelihood fit to the ΔE distribution sidebands ($|\Delta E| > 24$ MeV region indicated by the two vertical dashed lines in Fig. 2(a)). While normalizations are free parameters of the fit, the widths and means of the two Gaussian functions are fixed to the values obtained from a fit to the ΔE distribution of the misidentified data (Fig. 2(b)). The fit result is then integrated across the ΔE signal region (indicated by the two dotted lines in Fig. 2(a)) to obtain the number of background events,

TABLE I: Sources of systematic uncertainty in $\mathcal{B}(\overline{B}^0 \rightarrow D_s^- D^+)$ and $\mathcal{B}(\overline{B}^0 \rightarrow D_s^+ D_s^-)$ measurements.

Systematics	$\overline{B}^0 \rightarrow D_s^- D^+ [\%]$	$\overline{B}^0 \rightarrow D_s^+ D_s^- [\%]$
B 's of D_s and D mesons	10.1	18.6
Tracking	6.0	6.0
$PID(K^\pm/\pi^\pm)/K_S^0 \epsilon$	7.4	8.3
MC statistics	1.7	3.9
Signal window	1.0	2.1
Signal fraction $(1-r)$	2.9	
Fitting model	1.9	included in b
$N(B\overline{B})$	1.3	1.3
Total	14.5	21.7

$b = 6.7 \pm 0.8(\text{stat}) \pm 0.5(\text{syst})$, where the systematic error is evaluated by varying values of the fixed fit parameters by one standard deviation. Since only three events are observed in the ΔE signal region, the result for b indicates that there is no statistically significant signal present in this ΔE interval. Thus the expected 3.5% tail of the signal, which might populate the fitted region (parameterized as background only), can be safely neglected.

The average efficiency of the selection criteria $\epsilon(D_s D_s) = \sum_{i,j} \epsilon_{i,j} \mathcal{B}(D_{si}) \mathcal{B}(D_{sj}) = (2.45 \pm 0.46) \times 10^{-4}$ is evaluated from MC, where the intermediate branching fractions $\mathcal{B}(D_s \rightarrow \phi\pi)$ and $\mathcal{B}(D_s \rightarrow K^{*0}K)$ are taken from Ref. [16], and $\mathcal{B}(D_s \rightarrow K_S^0 K)$ is taken from Ref. [19].

To check for a possible peaking background we use events in the D_s mass sidebands. No peaking structures are observed in any of the $M_{bc}-\Delta E$ distributions.

V. RESULTS

We consider several sources of systematic uncertainty as listed in Table I. The largest contribution arises from an imprecise knowledge of the intermediate branching fractions of D_s and D mesons and amounts to $\pm 10.1\%$ ($\pm 18.6\%$) for $\overline{B}^0 \rightarrow D_s^- D^+$ ($\overline{B}^0 \rightarrow D_s^+ D_s^-$) decay mode [16, 19]. A 1% relative error for each of the charged tracks used in the reconstructed final states is assigned due to the uncertainty in tracking efficiency determined using partially reconstructed D^{*} 's. The particle identification efficiency has a relative uncertainty of 1.4% per charged kaon and 0.8% per charged pion, determined from $D^{*+} \rightarrow D^0 \pi^+$, $D^0 \rightarrow K^- \pi^+$ decays. The relative error for each reconstructed K_S^0 in the final state is 4.5%. A 1.7% (3.9%) uncertainty is due to the limited statistics of the MC sample used for the efficiency calculation. Since the efficiency is evaluated for the signal

region, we assign an additional 1% (2.1%) uncertainty due to the small possible difference in the signal resolution between data and MC samples. A 2.9% uncertainty is due to the imprecise knowledge of the fraction of true signal events, $(1-r)$, in the data sample. Systematic uncertainty arising from the description of the ΔE distribution is evaluated by comparing the known number of reconstructed $\overline{B}^0 \rightarrow D_s^- D^+$ events in the simulated sample with the fitted yield and is found to be 1.9%. Finally, the uncertainty in the number of $B\overline{B}$ events (1.3%) is taken into account. The sum in quadrature of the individual contributions gives a systematic error of 14.5% for a $\mathcal{B}(\overline{B}^0 \rightarrow D_s^- D^+)$ and 21.7% for a $\mathcal{B}(\overline{B}^0 \rightarrow D_s^+ D_s^-)$ measurement, excluding the uncertainty due to the fitting model included in b .

The number of signal $\overline{B}^0 \rightarrow D_s^- D^+$ events, $N_{D_s D}$, is converted into a branching fraction using the MC efficiency $\epsilon(D_s D)$ and the number of $B\overline{B}$ events. The measured branching fraction is given in Table II.

We use the world average of $\mathcal{B}(\overline{B}^0 \rightarrow D^+ \pi^-)$ [16] and calculate the ratio

$$R_{D_s/\pi}^{\text{ex.}} = \frac{\mathcal{B}(\overline{B}^0 \rightarrow D_s^- D^+)}{\mathcal{B}(\overline{B}^0 \rightarrow D^+ \pi^-)} = 2.65 \pm 0.42. \quad (1)$$

Before comparing this result to the numerical prediction of $R_{D_s/\pi}$ given in Ref. [6] — in which the calculation is performed in the generalized factorization scheme and includes penguin effects — we rescale it by a factor $(f_{D_s}^{\text{new}}/f_{D_s}^{\text{old}})^2$, where $f_{D_s}^{\text{new}}$ is the average value of D_s meson decay constant given in Refs. [16, 20] and $f_{D_s}^{\text{old}}$ is the value used in the original calculation. The expected value is $R_{D_s/\pi}^{\text{th.}} = 3.12 \pm 0.35$, where the uncertainty originates from the dependence on the decay constant f_{D_s} and form-factors, the former being the main source. The ratio $R_{D_s/\pi}^{\text{ex.}}/R_{D_s/\pi}^{\text{th.}} = 0.85 \pm 0.13(\text{ex.}) \pm 0.09(\text{th.})$ is consistent with unity. If one does not include the penguin contributions [6] to the amplitude for $\overline{B}^0 \rightarrow D_s^- D^+$ decay, the above ratio would be $0.61 \pm 0.10(\text{ex.}) \pm 0.07(\text{th.})$.

We observe no statistically significant signal in the $\overline{B}^0 \rightarrow D_s^+ D_s^-$ decay mode. The central value for the measured branching fraction is $[-3.4 \pm 1.6(\text{stat}) \pm 0.6(\text{syst}) \pm 0.6(B's)] \times 10^{-5}$. We infer an upper limit on the $\mathcal{B}(\overline{B}^0 \rightarrow D_s^+ D_s^-)$ from the total measured number of reconstructed events and the number of background events in the ΔE signal region ($n_0 = 3$ and $b = 6.7 \pm 0.9$, respectively), and the measured sensitivity, $S_0 = N_{B\overline{B}} \cdot \epsilon(D_s D_s) = (110 \pm 24) \times 10^3$. The latter error includes all systematic uncertainties given in Table I. To estimate the upper limit we use Bayes's theorem with a flat-prior for the signal following the prescription in (Section 32.3.1 in Ref. [16]):

$$p(\mathcal{B}|n_0, b, \sigma_b, S_0, \sigma_S) = \frac{\int_{-\infty}^{\infty} \int_{-\infty}^{\infty} L(n_0|\mathcal{B}, \mu_b) \mathcal{G}(S|S_0, \sigma_S) \pi(\mathcal{B}, \mu_b|b, \sigma_b) d\mu_b dS}{\int_{-\infty}^{\infty} \int_{-\infty}^{\infty} \int_{-\infty}^{\infty} L(n_0|\mathcal{B}', \mu'_b) \mathcal{G}(S'|S_0, \sigma_S) \pi(\mathcal{B}', \mu'_b|b, \sigma_b) d\mathcal{B}' d\mu'_b dS'}. \quad (2)$$

TABLE II: Results on the fitted numbers of events in the signal peak and branching fractions for $\overline{B}^0 \rightarrow D_s^- D^+$ decay mode. The peaking background fraction, r , is given for each D_s decay mode in the second column. The efficiencies include intermediate branching fractions ($\epsilon(D_s D) = \sum_j \epsilon_j \mathcal{B}(D_s) \mathcal{B}(D_j)$), which are taken for all three D and $D_s \rightarrow \phi \pi$ and $K^{*0} K$ decay modes from Ref. [16], and that for $D_s \rightarrow K_S^0 K$ is taken from Ref. [19]. In the last column the dominant sources of systematic uncertainty, the D_s branching fractions, $\mathcal{B}_{D_s X}$, are factored out. Quoted uncertainties for \mathcal{B} are statistical, systematic and uncertainty due to the imprecise knowledge of intermediate branching fractions, respectively.

Mode	N_{peak}	$r[\%]$	$\epsilon [10^{-4}]$	$\mathcal{B} [10^{-3}]$	$\mathcal{B} \cdot \mathcal{B}_{D_s X} [10^{-4}]$
$D_s^- \rightarrow \phi \pi^-, \phi \rightarrow K^+ K^-$	1112 ± 35	12.9 ± 4.5	2.8 ± 0.4	$7.8 \pm 0.2 \pm 0.9 \pm 1.0$	$1.68 \pm 0.05 \pm 0.19 \pm 0.06$
$D_s^- \rightarrow K^{*0} K^-, K^{*0} \rightarrow K^+ \pi^-$	961 ± 33	14.5 ± 4.3	2.5 ± 0.5	$7.3 \pm 0.3 \pm 0.8 \pm 1.5$	$1.83 \pm 0.06 \pm 0.21 \pm 0.07$
$D_s^- \rightarrow K_S^0 K^-, K_S^0 \rightarrow \pi^+ \pi^-$	441 ± 22	0.4 ± 2.2	1.3 ± 0.1	$7.3 \pm 0.4 \pm 0.9 \pm 0.6$	$0.76 \pm 0.04 \pm 0.09 \pm 0.03$
Combined	2514 ± 64	11.3 ± 2.6	6.6 ± 0.7	$7.5 \pm 0.2 \pm 0.8 \pm 0.8$	

The number of observed events n_0 is Poisson distributed around the sum of μ_s and μ_b : $L(n_0|\mu_s, \mu_b) = 1/n_0! (\mu_s + \mu_b)^{n_0} e^{-(\mu_s + \mu_b)}$, where μ_s and μ_b are the expected number of signal and background events, respectively. In particular μ_s can be written as $\mu_s = \mathcal{B} \cdot S$, where \mathcal{B} and S are true values of $\mathcal{B}(\overline{B}^0 \rightarrow D_s^+ D_s^-)$ and the sensitivity $N_{B_0 \overline{B}_0} \cdot \epsilon(D_s D_s)$, respectively. The true value of S can only take non-negative values and is Gaussian distributed around S_0 with variance σ_S . Hence $\mathcal{G}(S|S_0, \sigma_S)$ is a Gaussian function with a cut-off for $S < 0$. The prior probability density $\pi(\mathcal{B}, \mu_b|b, \sigma_b)$ is assumed to be factorizable, $\pi(\mathcal{B}, \mu_b|b, \sigma_b) = P(\mathcal{B})\mathcal{G}(\mu_b|b, \sigma_b)$. For $P(\mathcal{B})$ we use a flat-prior, and $\mathcal{G}(\mu_b|b, \sigma_b)$ is again a Gaussian function centered at b , with a width of σ_b and with a cut-off for $b < 0$.

Integrating out the nuisance parameters S and μ_b we obtain the posterior $p(\mathcal{B}|n_0, b, \sigma_b, S_0, \sigma_S)$, which already takes into account the statistical error on b , the systematic error due to the parameterization of ΔE distribution in the fit, and systematic uncertainties on the efficiency and on the number of $B\overline{B}$ pairs. The 90% C. L. upper limit on $\mathcal{B}(\overline{B}^0 \rightarrow D_s^+ D_s^-)$ following from this posterior is found to be

$$\mathcal{B}(\overline{B}^0 \rightarrow D_s^+ D_s^-) \leq 3.6 \times 10^{-5} \text{ at } 90\% \text{ C.L.}$$

VI. CONCLUSIONS

In conclusion, we have measured the branching fraction for $\overline{B}^0 \rightarrow D_s^- D^+$ decays. The measured value is $\mathcal{B}(\overline{B}^0 \rightarrow$

$D_s^- D^+) = [7.5 \pm 0.2(\text{stat}) \pm 0.8(\text{syst}) \pm 0.8(\mathcal{B}'\text{s})] \times 10^{-3}$, which represents a large improvement in accuracy as compared to previous measurements [7, 8, 9, 10]. Combining this result with the world average for $\mathcal{B}(\overline{B}^0 \rightarrow D^- \pi^+)$ [16] we obtain the ratio $R_{D_s/\pi}^{\text{ex.}}/R_{D_s/\pi}^{\text{th.}} = 0.85 \pm 0.13(\text{ex.}) \pm 0.09(\text{th.})$. With present experimental and theoretical uncertainties, the results are consistent with the factorization hypothesis for non-leptonic exclusive decays of B mesons. If one does not include the penguin contributions [6] to the amplitude for $\overline{B}^0 \rightarrow D_s^- D^+$ decay, the above ratio is not consistent with unity. For $\overline{B}^0 \rightarrow D_s^+ D_s^-$ decays we found no statistically significant signal. We set an upper limit of $\mathcal{B}(\overline{B}^0 \rightarrow D_s^+ D_s^-) \leq 3.6 \times 10^{-5}$ at 90% C.L. This result puts even more stringent limits on $\mathcal{B}(\overline{B}^0 \rightarrow D_s^+ D_s^-)$ than the recent measurement by the BaBar collaboration [21], severely challenges recent theoretical estimates in Refs. [4, 5] and implies that the weak annihilation contributions in decay modes with two charmed mesons are small, as suggested in Ref. [22].

We thank the KEKB group for excellent operation of the accelerator, the KEK cryogenics group for efficient solenoid operations, and the KEK computer group and the NII for valuable computing and Super-SINET network support. We acknowledge support from MEXT and JSPS (Japan); ARC and DEST (Australia); NSFC and KIP of CAS (China); DST (India); MOEHRD, KOSEF and KRF (Korea); KBN (Poland); MIST (Russia); ARRS (Slovenia); SNSF (Switzerland); NSC and MOE (Taiwan); and DOE (USA).

-
- | | |
|---|--|
| <p>[1] P. Krokovny <i>et al.</i> [Belle Collaboration], Phys. Rev. Lett. 89, 231804 (2002).</p> <p>[2] B. Aubert <i>et al.</i> [BABAR Collaboration], Phys. Rev. Lett. 90, 181803 (2003).</p> <p>[3] A. Drutskoy <i>et al.</i> [Belle Collaboration], Phys. Rev. Lett. 94, 061802 (2005).</p> <p>[4] Y. Li, C. D. Lu and Z. J. Xiao, J. Phys. G 31, 273 (2005).</p> <p>[5] J. O. Eeg, S. Fajfer and A. Prapotnik, Eur. Phys. J. C 42, 29 (2005).</p> | <p>[6] C. S. Kim, Y. Kwon, J. Lee and W. Namgung, Phys. Rev. D 65, 097503 (2002).</p> <p>[7] D. Bortoletto <i>et al.</i> [CLEO Collaboration], Phys. Rev. D 45, 21 (1992).</p> <p>[8] H. Albrecht <i>et al.</i> [ARGUS Collaboration], Z. Phys. C 54, 1 (1992).</p> <p>[9] D. Gibaut <i>et al.</i> [CLEO Collaboration], Phys. Rev. D 53, 4734 (1996).</p> <p>[10] B. Aubert <i>et al.</i> [BABAR Collaboration], Phys. Rev. D</p> |
|---|--|

- 74**, 031103 (2006).
- [11] A. Abashian *et al.* [Belle Collaboration], Nucl. Instrum. Meth. A **479**, 117 (2002).
- [12] S. Kurokawa and E. Kikutani, Nucl. Instrum. Meth. A **499**, 1 (2003), and other papers included in this Volume.
- [13] We use the EvtGen B -meson decay generator developed by the CLEO and BaBar Collaborations, see: <http://www.slac.stanford.edu/~lange/EvtGen/>. The detector response is simulated by a program based on GEANT-3, CERN program library writeup W5013, CERN, (1993). A small fraction of events are generated with the CLEO QQ generator, see: <http://www.lns.cornell.edu/public/CLEO/soft/qq>. For these events the detector response is also simulated with GEANT, R. Brun *et al.*, GEANT 3.21, CERN Report DD/EE/84-1, 1984.
- [14] Z. Natkaniec *et al.*, [Belle SVD2 Group] Nucl. Instrum. Meth. A **560**, 1 (2006).
- [15] E. Nakano, Nucl. Instrum. Meth. A **494**, 402 (2002).
- [16] W.-M. Yao *et al.* [Particle Data Group], J. Phys. G **33**, 1 (2006).
- [17] G. C. Fox and S. Wolfram, Phys. Rev. Lett. **41**, 1581 (1978).
- [18] A. Drutskoy *et al.* [Belle Collaboration], Phys. Lett. B **542**, 171 (2002).
- [19] N. Adam *et al.* [CLEO Collaboration], arXiv:hep-ex/0607079.
- [20] M. Artuso *et al.* [CLEO Collaboration], arXiv:hep-ex/0607074.
- [21] B. Aubert *et al.* [BABAR Collaboration], Phys. Rev. D **72**, 111101 (2005).
- [22] C. H. Chen, C. Q. Geng and Z. T. Wei, Eur. Phys. J. C **46**, 367 (2006).